Proceedings of the 34th Annual Mechanism and Robotics Conference
IDETC/CIE 2010
August 15-18, 2010, Montreal, Canada

DETC2010-28750

EVALUATION OF CONTACT FORCE AND ELASTIC FOUNDATION MODELS FOR WEAR ANALYSIS OF MULTIBODY SYSTEMS

Saad M. Mukras
Mechanical Engineering
Qassim University
Buraydah, Qassim, Saudi Arabia
mukras@qec.edu.sa

Nathan A. Mauntler
Mechanical & Aerospace Eng.
University of Florida
Gainesville, Fl, 32611
mauntler@ufl.edu

Nam Ho Kim
Mechanical & Aerospace Eng.
University of Florida
Gainesville, Fl, 32611
nkim@ufl.edu

Tony L. Schmitz
Mechanical & Aerospace Eng.
University of Florida
Gainesville, Fl, 32611
tschmitz@ufl.edu

W. Gregory Sawyer
Mechanical & Aerospace Eng.
University of Florida
Gainesville, Fl, 32611
wgsawyer@ufl.edu

ABSTRACT

In this paper, two procedures to analyze planar multibody systems experiencing wear at a revolute joint are compared. In both procedures, the revolute joint of interest includes a clearance whose shape and size are dictated by wear. The procedures consist of coupled iterative analyses between a dynamic analysis of the system with non-ideal joints and wear prediction to determine the evolution of the joint clearance. In the first procedure, joint forces and contact pressure are estimated using the elastic foundation model (EFM) with hysteresis damping via the dynamic analysis. In the second procedure, a contact force model with hysteresis damping is used to estimate the joint forces. In the latter case, however, the contact pressure is estimated using a finite element method (FEM). Comparison in performance of the two models is facilitated through the use of an experimental slider-crank mechanism in which wear is permitted to occur at one of the joints. It is observed that the two procedures provide similar estimates for the dynamics response and wear volumes but substantially different predictions on the wear profiles. Additionally, experimental results show that while predictions on the wear volume from both models are reasonably accurate, the FEM-based model produced more accurate predictions on the wear profile.

1. INTRODUCTION

Mechanical/multibody systems consist of a number of components that are interconnected by joints. These joints typically consist of at least two components that are in contact and experience relative motion. It is therefore inevitable that joint wear will occur. Depending on the system configuration and the amount of wear at the joints, the performance of the system may be adversely affected. It is therefore no surprise that a considerable amount of effort has been expended to develop ways to account for wear in the design process. One approach is to develop procedures that can be used to estimate wear beforehand. A trend that has developed, in this regard, is the use of Archard's [1] wear model in an iterative wear prediction scheme. In this scheme, incremental wear is estimated based on the relative sliding, the contact pressure and tribological data (typically in the form of a wear coefficient) that describes the operating conditions. The geometry is then updated to reflect wear and the incremental wear is recomputed and accumulated in subsequent iterations. This procedure has been used in a number of applications including wear prediction in cam and follower components [2-5], revolute joint components [6], helical gears [7] and spur gears [8, 9]. It has also been used in medical applications to predict wear in hip arthroplasty [10, 11].

Despite the increasing use of the iterative wear prediction procedure, for certain cases the procedure may yield less than accurate predictions. This is because the procedure is a component level prediction in which the component is isolated from the entire system and the wear estimate is based on initial system dynamics. Two possible errors may be associated with the component level assumption. First, as the wear at the

contact interface of the component evolves, the system dynamics may also evolve. Thus, the joint forces responsible for the wear are altered as the wear progresses. Depending on the degree of evolution, it may not be sufficient to use the initial dynamics in the wear prediction. This issue was identified and documented by Blanchet [12] and Sawyer [13] for a scotch yoke mechanism and by Dickrell et al. [14] for cam wear. Secondly, without performing a dynamic analysis it may not be possible to correctly determine the contact locations in the joint and the predictions may lead to incorrect wear profiles. This aspect of wear prediction was also identified and discussed by Mukras et al. [15] and Flores [16]. In Mukras et al. [15], a procedure to analyze multibody systems with non-ideal joints based on a contact force model was coupled with the previously discussed wear prediction procedure. This coupling accounts for changes in the dynamics due to joint wear. In addition, the contact locations and, subsequently, the wear regions can be predicted in a multibody dynamic framework. The procedure was used to estimate the wear at a revolute joint in a slider-crank mechanism. Results from the model showed agreement with experiment. A similar procedure was presented by Flores [16].

In this paper, a procedure to analyze planar multibody systems with revolute joint wear, similar to that used in Mukras et al. [15] and Flores [16], is presented. However, the procedure is based on the elastic foundation model (EFM), rather than the contact force model. A similar concept was employed by Bei et al. [17] in multibody analysis of knee contact and by Fregly et al. [18] in wear prediction of a knee replacement. The procedure presented here employs the EFM to simultaneously estimate the joint reaction force, required in the dynamic analysis, and contact pressure distribution at the joint, which is required for wear analysis. The EFM-based procedure is then compared with the contact force model approach. The advantages and disadvantages of the two procedures are then discussed. The aim of this paper is to present a fair comparison between the two procedures to enable users the opportunity to make an informed choice.

2. WEAR PREDICTION PROCEDURE

In this work, an iterative wear prediction procedure, similar to the one used in the works of Podra et al. [19, 20], is employed. The procedure is based on Archard's wear model which can be expressed in differential form as follows:

$$\frac{dh}{ds} = kp(s). \tag{1}$$

In Eq. (1), h is the wear depth, s and p are the relative sliding distance and contact pressure between the contacting bodies and k is the wear coefficient. If the two bodies are made of different materials, each body will have a separate wear coefficient. The wear depth may be estimated using a finite difference approach in which a temporal discretization of the relative motion of the bodies in contact yields the following updating formula:

$$h_i = h_{i-1} + kp_i \Delta s_i . \tag{2}$$

In Eq. (2), p_i, h_i and Δs_i are the contact pressure, wear depth and incremental sliding distance at the i^{th} cycle and h_{i-1} is the wear depth at the previous cycle. The product on the right-hand side of Eq. (2) is referred to as the incremental wear depth. In this term, the incremental sliding distance is usually specified while the wear coefficient is determined through experiments [21–23] and the contact pressure is determined using numerical techniques such as EFM or the finite element method (FEM).

Accurate wear predictions require that the geometry be updated to reflect the evolving contact conditions. One way to achieve this is by displacing the contact boundary in the direction of the surface normal by an amount equal to the wear estimated by Eq. (2). In addition, these procedures must incorporate some strategies, such as extrapolation, to minimize computational costs. More detailed studies on wear prediction on geometries, such as the revolute joints including geometry update and the use of extrapolations, can be found in Mukras et al. [6] and Kim et al. [21].

3. ANALYSIS OF MULTIBODY SYSTEMS

In order to predict joint wear within a system, it is necessary to formulate it within the multibody dynamic analysis of the system. The analysis of multibody systems with either ideal or non-ideal joints involves the assembly and solution of a set of differential algebraic equations of motion (DAE). A brief discussion on how to perform a dynamic analysis is presented in this section.

A multibody system consists of several components (bodies) that are interconnected by joints which impose restrictions on the relative motion of the bodies. The description of interconnections is expressed through algebraic equations known as kinematic constraints. The kinematic constraint can be expressed as [24, 25]:

$$\mathbf{\Phi}(\mathbf{q}, t) = \mathbf{0}, \tag{3}$$

where $\mathbf{q}$ is the set of generalized coordinates that uniquely define the position and orientation of all bodies in the system and t is time. Equation (3) is usually referred to as the position equation. It is differentiated once to obtain the velocity equation and twice for the acceleration equation. These equations can, respectively, be expressed as:

$$\mathbf{\Phi}_{\mathbf{q}}\dot{\mathbf{q}} = -\mathbf{\Phi}_{t}, \tag{4}$$

$$\mathbf{\Phi}_{\mathbf{q}}\ddot{\mathbf{q}} = -\left(\mathbf{\Phi}_{\mathbf{q}}\dot{\mathbf{q}}\right)_{\mathbf{q}}\dot{\mathbf{q}} - 2\mathbf{\Phi}_{\mathbf{q}t}\dot{\mathbf{q}} - \mathbf{\Phi}_{tt} \equiv \boldsymbol{\gamma} . \tag{5}$$

For a properly constrained system, Eqs. (3), (4) and (5) can be solved to determine the position, velocity and acceleration of the system components. This analysis, referred to as a kinematic analysis, provides only information on the motion of the system. A dynamic analysis is required in order to determine the

dynamic response of a multibody system. This involves formulating and solving the DAE of motion. The DAE can be obtained by combining the equations of motion for the system and the acceleration equation (Eq. (5)). For a constrained rigid multibody system, the equation on motion for a multibody system can be expressed as [24, 25]:

$$\mathbf{M}\ddot{\mathbf{q}} + \mathbf{\Phi}_{\mathbf{q}}^{T}\boldsymbol{\lambda} = \mathbf{Q}^{A}, \tag{6}$$

where $\mathbf{M}$ is the generalized mass matrix consisting of masses and moments of inertia for the system components, $\ddot{\mathbf{q}}$ and $\mathbf{\Phi}_{\mathbf{q}}^{T}$ are the generalized acceleration vector and Jacobian of the constraints, respectively, $\boldsymbol{\lambda}$ is a vector of Lagrange multipliers, and $\mathbf{Q}^{A}$ is a vector of externally applied loads. The second term on the left hand side of Eq. (6) is the vector of reaction forces. For an unconstrained system, the vector of Lagrange multipliers is zero and this term disappears.

Equations (5) and (6) can then be combined to result in a mixed system of differential algebraic equations (DAE) of motion. The equations are expressed as:

$$\begin{bmatrix} \mathbf{M} & \mathbf{\Phi}_{\mathbf{q}}^{T} \\ \mathbf{\Phi}_{\mathbf{q}} & \mathbf{0} \end{bmatrix} \begin{bmatrix} \ddot{\mathbf{q}} \\ \boldsymbol{\lambda} \end{bmatrix} = \begin{bmatrix} \mathbf{Q}^{A} \\ \boldsymbol{\gamma} \end{bmatrix}. \tag{7}$$

Equation (7) can then be solved to reveal the dynamics of the system. The solution procedure for this equation is well documented in the literature [24–26].

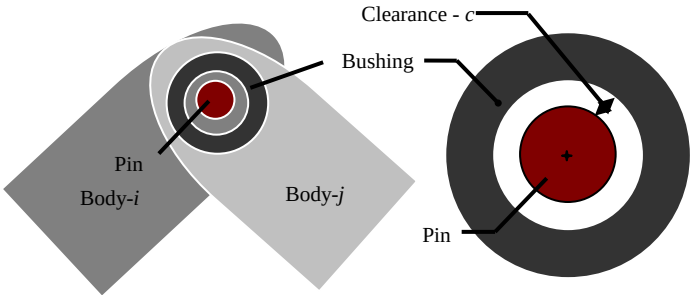

Figure 1: A revolute joint with clearance.

4. ANALYSIS OF MULTIBODY SYSTEMS WITH NON-IDEAL JOINTS

In this section the procedure to model non-ideal revolute joints using the contact force model and the EFM is presented. The analysis of a system with such joints can then be performed with the procedure outlined in section 3.

It is assumed in this work that the revolute joint consists of two components, a pin and a bushing. The pin and the bushing are rigidly attached to the two bodies that share the joint. This is depicted in Fig. 1 where the pin and the bushing are, respectively, attached to body i and body j. The ideal revolute joint, which allows relative rotation between two bodies in the system, assumes that no clearance is present at the joint and the pin and bushing center coincide at all time. In the case of a non-ideal revolute joint, clearance is present at the joint so that the pin and bushing centers do not necessarily coincide.

The joint components (pin and bushing) of a non-ideal joint can assume one of three configurations. The three configurations are: freefall, when the components are not in contact; impact, when contact is established; and the following motion, which together describe the duration when the joint components are in contact and in relative motion. It is possible to model the effect of a non-ideal joint by ensuring that the motion of the pin is confined within the inner perimeter of the bushing. This can be achieved by using a force constraint in place of a kinematic constraint to describe the joint. The force constraint involves applying a force on the joint components every time contact is established (this force is equivalent to the joint reaction). This procedure has previously been used by Ravn [27] and Flores et al. [28].

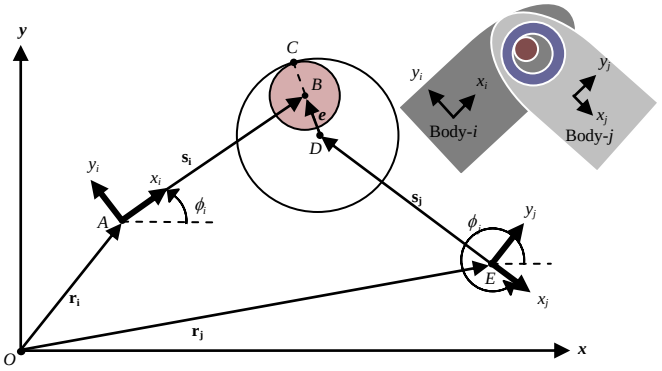

Figure 2: Geometric description of a non-ideal revolute joint with eccentric vector e.

Before the constraint/contact force can be applied, it is necessary to determine the direction in which the contact force is acting. In Fig. 2, a diagram of two bodies constrained by a non-ideal revolute joint is shown. Body coordinates x_i-y_i and x_j-y_j are fixed to the center of masses of the bodies i and j, respectively. The coordinates are oriented at angles ϕ_i and ϕ_j relative to the global x-axis. The point of contact C is defined as the center of contact region between the pin and the bushing. This point can be located using the eccentric vector e which is a vector connecting the bushing center D and the pin center B. At the time of contact the eccentric vector points in the direction of the contact. It is assumed that this is also the direction in which the joint reaction will act. This vector is expressed as:

$$\mathbf{e} = \left(\mathbf{r}_i + \mathbf{A}_i\mathbf{s}_i\right) - \left(\mathbf{r}_j + \mathbf{A}_j\mathbf{s}_j\right), \tag{8}$$

where $\mathbf{r}_i$ and $\mathbf{r}_j$ are vectors linking the global origin and the center or masses of the bodies, $\mathbf{s}_i$ and $\mathbf{s}_j$ are vectors in the local coordinate system that link the center of masses to the pin and bushing centers respectively, and $\mathbf{A}_i$ and $\mathbf{A}_j$ are matrices that transform a vector from the local coordinate system to the global system. In this case, they transform vectors $\mathbf{s}_i$ and $\mathbf{s}_j$

into their global equivalent. A unit vector in the direction of the eccentric vector can be defined by:

$$\mathbf{n} = \frac{\mathbf{e}}{e}; \quad e = \|\mathbf{e}\|. \tag{9}$$

The constraint/contact force can then be applied in the direction of the above unit vector. The forces can be estimated using a contact form model with hysteresis damping [29] as discussed by Ravn [27] and Flores et al. [28]. The EFM may also be used to determine the constraint force. The two techniques will be discussed in the following subsections.

4.1. Contact Force Model for Modeling Non-Ideal Revolute Joints

It is assumed that, while the joint components are compliant, the bodies to which the components are attached are rigid. It is then possible to estimate the constraint force using a contact force model. A widely used model in multibody analysis, which was derived for colliding spheres, is the Hertz model with hysteresis damping [29]. It assumes a nonlinear relation between the contact force and the penetration δ resulting from the contact. Using this model, the force normal to the plane of contact can be expressed as:

$$F_N = K\delta^n + D\dot{\delta}, \tag{10}$$

where n = 1.5 and K is a constant that represents compliance. The constant K depends on the elastic constants υ and E as well as the radii (R_i and R_j) of the spheres:

$$K = \frac{4}{3\left(b_i + b_j\right)} R^{\frac{1}{2}}, \tag{11}$$

where

$$R = \left(\frac{R_i R_j}{R_i + R_j} \right); \qquad b_k = \frac{1-\upsilon_k^2}{E_k}; \qquad k = i, j. \tag{12}$$

In the case of conformal contact as shown in Fig. Figure 2, the radius of the second body (R_j) should take a negative value. Damping is included in the contact model in the form of a damping coefficient D and the penetration velocity $\dot{\delta}$. The damping coefficient is expressed as:

$$D = \frac{3K\left(1-e_r^2\right)}{4\dot{\delta}^{(-)}} \delta^n, \tag{13}$$

where e_r and $\dot{\delta}^{(-)}$ are the coefficient of restitution and the initial penetration velocity upon impact.

The coefficient of restitution plays an important role when components impact at high relative velocities resulting in bouncing of the components and elasto-plastic deformation [44, 45]. However, in the revolute joint, the interaction between the joint components is mainly smooth contact with continuous sliding. The contact surface will experience only elastic deformation. In such a case, the effect of the coefficient of restitution is minimal.

The model described by Eq. (10) is valid for colliding spheres whose contact area is small and circular. While several expressions have been proposed to model the colliding cylinders [30, 31] (as is the case for revolute joints), this model (Eq. (10)) has been used in multibody dynamic analysis by a number of researchers [27, 28, 32] to estimate the contact force between colliding cylinders. In addition, the Hertz contact model may lead to erroneous results when the conformity is large [43]. The justifications for using the expression in Eq. (10) are that (1) the depth of revolute joint is relatively small compared to the diameter of the joint and (2) the error in Eq. (10) is acceptable as long as the contact force is calculated accurately from the dynamic analysis because the penetration will be re-calculated from either the EFM or FEM model. A more detailed discussion of the justification is presented in the literature [26–28]. In this work, Eq. (10) is thus used to estimate the contact force at the revolute joint. It will be shown that this approach yields similar results to experiment when used in multibody analysis.

In order to evaluate the contact force in Eq. (10), the penetration has to be determined. In the case of the non-ideal revolute joint, the penetration between the pin and bushing during contact is computed as the difference between the eccentricity and clearance:

$$\delta = e - c, \tag{14}$$

where the clearance is defined as the difference between the bushing and pin radii, $c = R_j - R_i$. When the pin and bushing are not in contact, the eccentricity is smaller than the clearance and the penetration has a negative value. However, when the value of the penetration is equal to or greater than zero, contact is established. Thus, for a value of δ greater than zero, a contact force is applied between the bodies. The contact force vanishes when δ is equal to or less than zero.

Estimates of the joint forces may be enhanced by including friction. In this work, Coulomb friction is applied. The friction force is expressed as:

$$F_f = \mu_k F_N, \tag{15}$$

where μ_k is the coefficient of friction which can be determined through experiments as discussed by Schmitz [33] and F_N is the normal force as defined in Eq. (10).

4.2. EFM for Modeling Non-Ideal Revolute Joints

In the EFM the contact surface is modeled as a set of springs (spread over the contact surface). The springs represent the elastic layer and the thickness of the layer is composed of the thickness of one or both bodies (depending on whether one of the bodies is defined as rigid).

The EFM assumes that the springs are independent from each other and thus the shear force between them is neglected. The consequence of this assumption is that the model does not account for how pressure applied at one location affects the deformation at other locations. This is contrary to what is experienced in elastic contact where the displacement at one location is a function of the pressure applied at other locations. Although this simplifying assumption violates the very nature of contact problems, some benefits can be derived from its use. In particular, the simplified model provides a cheaper alternative for estimating contact pressure (compared to other computational techniques such as the FEM) and facilitates the analysis of conformal geometry, layered contact and nonlinear materials [17].

The contact pressure for any spring (spring i) in the elastic foundation can be calculated from [19]:

$$p_i = \frac{E_W}{L_i}\delta_i, \tag{16}$$

where p_i is the contact pressure, E_W is the elastic modulus for the elastic layer, L_i is the thickness of the elastic layer and δ_i is the deformation of the spring. When both bodies are deformable E_W is a composite of the elastic modulus and Poisson's ratio for the two bodies. The procedure to determine the composite modulus is discussed by Podra [19] and in more detail by Johnson [34]. For the purpose of illustration, it is assumed that only one of the bodies in contact is deformable. For this case, a common expression for E_W is given by [17, 18, 35-38]:

$$E_W = \frac{(1-\upsilon)E}{(1+\upsilon)(1-2\upsilon)}, \tag{17}$$

where E and υ are the elastic modulus and Poisson's ratio of the deformable body, respectively. The contact pressure for the spring i can then be determined from:

$$p_i = \frac{(1-\upsilon)E}{(1+\upsilon)(1-2\upsilon)}\frac{\delta_i}{L_i}, \tag{18}$$

The total load supported by the elastic layer (or the joint reaction force) can then be computed by summing the contact forces on all elements in the direction of the mid-surface normal. The resultant force has a magnitude equal to the joint reaction with direction normal to the contact plane (as defined in Eq. (9)). The magnitude of the resultant can be expressed as the sum of the product of the element pressure p_i and the element area A_i projected in the direction of load application n (or direction of eccentric vector; see Eq. (9)):

$$F_N = \sum p_i A_i . \tag{19}$$

In the case of the revolute joint, the element area in Eq. (19) can be estimated using the following expression:

$$A_i = \left(\frac{1}{2}R_{pin}^2\theta_i\right)d_{bushing} . \tag{20}$$

where R_{pin} is the pin radius, $d_{bushing}$ is the bushing depth and θ_i is the angle between two discretized points on the bushing measured from the pin center.

To enable a fair comparison between the contact force model and EFM, a damping term, similar to the one used in the contact force model, should be added to Eq. (19). The EFM model with damping can be derived by noting that individual spring force without damping can be expressed as:

$$F_{N_i} = p_i A_i, \tag{21}$$

The contact pressure in Eq. (18) can be substituted into Eq.(21) to result in the following expression for the individual spring force:

$$\begin{aligned} F_{N_i} &= \frac{(1-\upsilon)E}{(1+\upsilon)(1-2\upsilon)}\frac{A_i}{L_i}\delta_i, \\ &= KA_i \end{aligned} \tag{22}$$

where the spring constant K is

$$K = \frac{(1-\upsilon)E}{(1+\upsilon)(1-2\upsilon)}\frac{\delta_i}{L_i} . \tag{23}$$

The EFM model with damping can then be expressed as:

$$\begin{aligned} F_{N_i} &= K\delta_i + D\delta_i \\ &= K\delta_i + K\frac{3\left(1-e_r^2\right)}{4\dot{\delta}^{(-)}}\dot{\delta}\delta_i \\ &= \frac{(1-\upsilon)E}{(1+\upsilon)(1-2\upsilon)}\frac{A_i}{L_i}\delta_i + \frac{(1-\upsilon)E}{(1+\upsilon)(1-2\upsilon)}\frac{A_i}{L_i}\frac{3\left(1-e_r^2\right)}{4\dot{\delta}^{(-)}}\dot{\delta}\delta_i \\ &= \frac{(1-\upsilon)E}{(1+\upsilon)(1-2\upsilon)}\frac{\delta_i}{L_i}A_i + \frac{(1-\upsilon)E}{(1+\upsilon)(1-2\upsilon)}\frac{\delta_i}{L_i}\frac{3\left(1-e_r^2\right)}{4\dot{\delta}^{(-)}}\dot{\delta}A_i \end{aligned} \tag{24}$$

Noting that the contact pressure is given by Eq.(18), Eq.(24) can be written as:

$$F_{N_i} = p_i A_i + p_i A_i\left(\frac{3\left(1-e_r^2\right)}{4\dot{\delta}^{(-)}}\right)\dot{\delta} . \tag{25}$$

The total contact force can then be obtained as the sum of the individual forces. The contact force can then be expressed as:

$$F_N = \sum \left(p_i A_i + p_i A_i \left(\frac{3\left(1-e_r^2\right)}{4\dot{\delta}^{(-)}} \right) \dot{\delta} \right). \tag{26}$$

Once the contact forces are determined using either of the two procedures (contact force model or EFM), they may be assembled into the DAE (Eq. (7)) as applied loads. The DAE may then be solved to reveal the system dynamics.

4.3. Example: Slider-Crank Mechanism with Joint Clearance

The slider-crank mechanism shown in Fig. Figure 3 is used to illustrate the procedure to model planar systems with non-ideal revolute joints. The mechanism consists of two ideal revolute joints, one between the ground and the crank and the other between the follower and the slider, a non-ideal joint between the crank and the follower and an ideal translational joint between the slider and the ground. The dimension and mass properties of the slider-crank are listed in Table Table 1. In Table If it is assumed that the crank is driven at a constant angular velocity of ω the kinematic constraints can be formulated using methods discussed in Nikravesh [24] and Haug [25]. For this system, the kinematic constraints can be written as:

$$\mathbf{\Phi} = \begin{bmatrix} x_1 - l_1\cos\phi_1 \\ y_1 - l_1\sin\phi_1 \\ x_2 - x_3 + l_2\cos\phi_2 \\ y_2 - y_3 - l_2\sin\phi_2 \\ y_3 \\ \phi_3 \\ \phi_1 - \omega t \end{bmatrix} = \begin{bmatrix} 0 \\ 0 \\ 0 \\ 0 \\ 0 \\ 0 \\ 0 \end{bmatrix}, \tag{27}$$

where l_1 and l_2 are the lengths of the crank and the follower and x_i, y_i and ϕ_i are the generalized coordinates. In Eq. **Error!** the first four equations describe the two ideal revolute joints, the 5th and 6th equations represent the translational joint and the last equation describes the driving constraint that specifies the velocity of the crank. It should be emphasized that, since the joint between the crank and the follower is non-ideal, it does not appear in the set of kinematic constraints. The non-ideal joint is instead described using a force constraint that is present in the DAE as applied loads.

Table 2, the material properties and dimensions for the joint components are provided. The pin and bushing are assumed to be made of steel and polytetrafluoroethylene (PTFE), respectively.

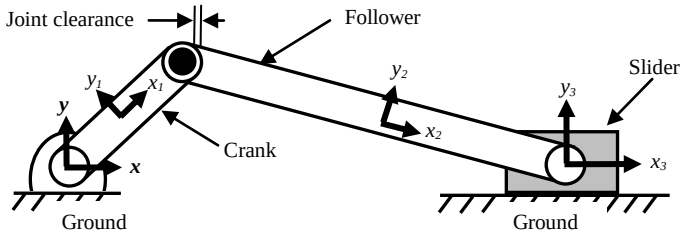

Figure 3: Slider-crank mechanisms with joint clearance between the crank and follower.

Table 1: Dimension and mass parameter for slider-crank mechanism

	Length (m)	Mass (g)	Moment of inertia (kg-m^2)
Crank	1.00	10.00	45.00
Connecting Rod	1.75	15.00	35.00
Slider	--	30.00	--

If it is assumed that the crank is driven at a constant angular velocity of ω the kinematic constraints can be formulated using methods discussed in Nikravesh [24] and Haug [25]. For this system, the kinematic constraints can be written as:

$$\mathbf{\Phi} = \begin{bmatrix} x_1 - l_1\cos\phi_1 \\ y_1 - l_1\sin\phi_1 \\ x_2 - x_3 + l_2\cos\phi_2 \\ y_2 - y_3 - l_2\sin\phi_2 \\ y_3 \\ \phi_3 \\ \phi_1 - \omega t \end{bmatrix} = \begin{bmatrix} 0 \\ 0 \\ 0 \\ 0 \\ 0 \\ 0 \\ 0 \end{bmatrix}, \tag{27}$$

where l_1 and l_2 are the lengths of the crank and the follower and x_i, y_i and ϕ_i are the generalized coordinates. In Eq. **Error! Reference source not found.** the first four equations describe the two ideal revolute joints, the 5th and 6th equations represent the translational joint and the last equation describes the driving constraint that specifies the velocity of the crank. It should be emphasized that, since the joint between the crank and the follower is non-ideal, it does not appear in the set of kinematic constraints. The non-ideal joint is instead described using a force constraint that is present in the DAE as applied loads.

Table 2: Material properties and dimensions for the joint components

	Pin (steel)	Bushing (PTFE)
Young's modulus	206.8 GPa	0.5 GPa
Poisson ratio	0.29	0.38
Radius	20 mm	20.0003, 23 mm

The DAE for this system can easily be assembled and solved. For a crank speed of 30 rpm, representative results of the dynamic analysis are shown in Figures 4–7. In Fig. 4, comparisons of the joint reaction between the ideal and non-ideal joints are provided for two clearance sizes when the contact force model is used. For a clearance of 0.0003 mm the two cases predict almost identical values for the joint reaction Fig. 4(a)). This similarity in joint reaction predictions is expected since the clearance is small enough so that the non-ideal joint behaves essentially like an ideal joint. In Fig. 4(b), a plot of the joint reaction of the non-ideal joint for a clearance of 3 mm is shown. From the two plots it is clear that as the clearance is increased, the curve of the joint reaction evolves from a smooth one to one characterized by peak forces. The location of these peaks can be explained by noting that they occur right after the joint reaction attains a minimum value or when contact between the joint components is temporarily lost. When contact is reestablished, there is an impact which causes the peaks forces. Similar results are obtained when the EFM is used to model the non-ideal joint except that higher peak forces are observed (see Fig. 5).

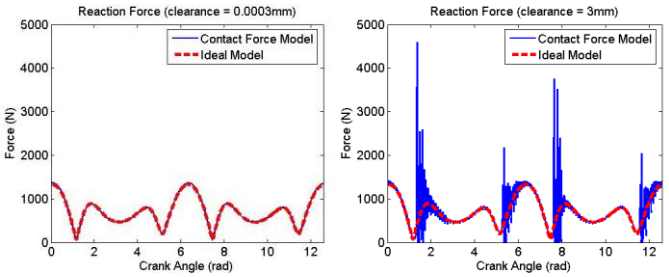

a b

Figure 4: Comparison of reaction between the ideal and the non-ideal joints for various joint clearances for the contact force model.

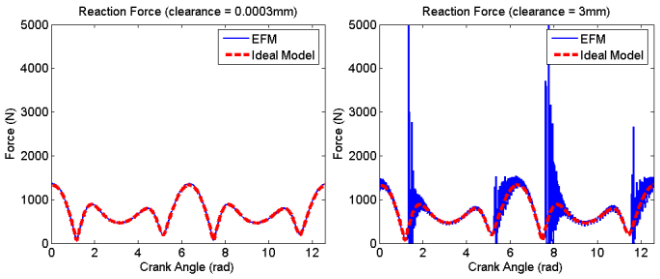

a b

Figure 5: Comparison of reaction between the ideal and the non-ideal joints for various joint clearances for EFM.

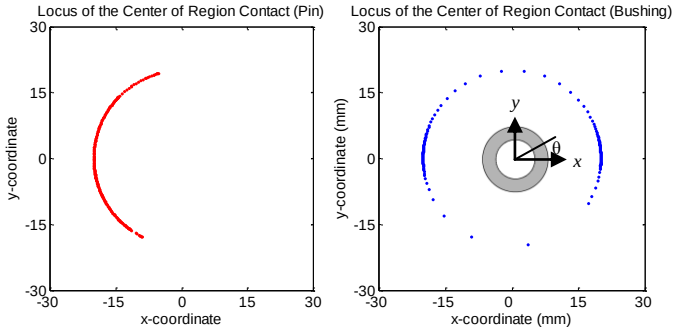

a b

Figure 6: Locus of contact point '*C*' for a complete crank cycle based on the contact force model. a) Locus for the pin. b) Locus for the bushing.

In Fig. 6(a), the locus of the center points of the contact region (contact point '*C*' as defined in Fig. Figure 2) for a complete crank cycle, measured from the pin center, is shown. The corresponding locus of points for the bushing, measured from the bushing center, is shown in Fig. 6(b). For the pin (Fig. 6(a)), the locus contact points '*C*' are concentrated on the left half, whereas for the bushing (Fig. 6(b)) the contact point '*C*' is concentrated on both the left and the right side of the bushing. This corresponds to bushing angular coordinates of approximately 0 and π radians as defined in Fig. 6(b). Similar results are obtained when the non-ideal joint is modeled using the EFM procedure (Fig. 7).

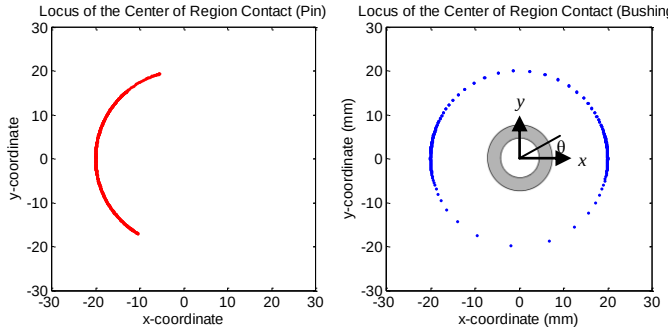

a b

Figure 7: Locus of contact point '*C*' for a complete crank cycle based on EFM. a) Locus for the pin. b) Locus for the bushing.

The importance of the point '*C*' cannot be overemphasized. This point is a reference point in the dynamic analysis when using the previously outlined procedures to model systems non-ideal revolute joints. It identifies the locations where the constraint force will be applied and thus the regions that will experience wear. It would be difficult to predetermine the locations that would wear without knowledge of this point; this highlights the need for a system level wear prediction.

5. WEAR ANALYSIS OF MULTIBODY SYSTEMS WITH NON-IDEAL REVOLUTE JOINT

In section 2, a procedure to predict wear at the interface of two bodies that are in contact and relative motion was presented. Later, two dynamic analysis procedures to analyze multibody systems with non-ideal revolute joints were discussed. Next, the dynamic analysis procedures and the wear prediction procedure must be integrated to enable the analysis of multibody systems with joint wear. This type of analysis allows any changes in the system dynamics caused by joint wear to be captured. In addition, the analysis allows the correct contact location (where wear occurs) to be identified in accordance with the wear prediction procedure.

In the integrated model, previously discussed in Mukras et al. [15], a dynamic analysis is performed on the system for a complete cycle in order to determine the joint reactions as well as the incremental siding distance at the wearing joints. This information is obtained at each time increment of the discretized cycle. Thus, for a non-ideal joint b, the contact and friction force at time increment ti can be expressed as:

$$\begin{aligned} \mathbf{F}^{b}_{N,t_i} &= F_{N,t_i}\mathbf{n}_{,t_i} \\ \mathbf{F}^{b}_{\mu,t_i} &= \mu_k F_{N,t_i}\mathbf{n}_{,t_i}{}^{\perp} \end{aligned}, \tag{28}$$

where F_N is the contact force determined via the contact force model or EFM and $\mathbf{n}$ is a unit normal vector pointing in the direction of contact. The corresponding incremental sliding distance can also be described as:

$$\Delta s_{t_i} = R_j \bullet \left(\alpha_{t_i} - \alpha_{t_{i-1}}\right), \tag{29}$$

where R_j is the bushing radius, α_{t_i} is the angular difference (in radians) between the local x- axes of the two bodies *i* and *j* that share the revolute joint at a current time, and $\alpha_{t_{i-1}}$ corresponds to the difference at a previous time.

The joint reaction and the incremental sliding distance can then be used to estimate the joint wear using the procedure outlined is section 2. It is, however, necessary to first determine the contact pressure distribution at the joint. For the dynamics analysis procedure based on the EFM, the contact pressure is readily available from the dynamic analysis, whereas for the contact force based procedure, FEM is used to determine the contact pressure distribution. The wear is estimated using Eq. (2) and the geometry is updated to reflect the wear. The evolving geometry must also be reflected in the dynamic analysis. This can be done by noting that the value of the clearance c will no longer be a constant but will depend on the contact point '*C*' as defined in Fig. Figure 2. The new value for the clearance c can be determined by the following expression:

$$c = \left\| \mathbf{r}_B - \mathbf{r}_D \right\|, \tag{30}$$

where $\mathbf{r}_B$ and $\mathbf{r}_D$ are the position vectors of the pin and bushing centers, respectively. In the case of the contact force model, once the value of the clearance c at the reference contact point '*C*' has been obtained (using Eq. (30)), the new value of R_j at contact point '*C*' can be determined using the expression $c = R_j - R_i$ (see Eq. (14)). In this case it is assumed that the value of R_i remains constant. The contact force model can then be updated for with new value of R_j. In the case of the EFM, the new value of the clearance c at the reference contact point '*C*' is also obtained using Eq. (30). The penetration at that point can then be obtained using Eq. (14).

Once the pin and bushing geometries have been updated and the clearance size is adjusted to reflect the wear, a dynamic analysis for the next cycle is performed. The wear is then computed based on the results of the new dynamic analysis followed by an update on the geometry and clearance size. This process is repeated until the desired number of cycles has been completed. Flowcharts showing the integrated models based on the contact force model and the EFM model are shown in Fig. 8 and Fig. Figure 9, respectively.

6. COMPARISON BETWEEN THE EFM AND A CONTACT FORCE MODEL IN WEAR ANALYSIS OF MULTIBODY SYSTEMS

Two procedures to analyze multibody systems with joint wear were presented in section 5. In this section the two procedures are used to simulate an actual slider-crank mechanism in which wear is allowed to occur at one of the joints. The wear results from the two procedures are compared. In addition, the performance of the two procedures is assessed by comparing simulation results to results from the actual mechanism.

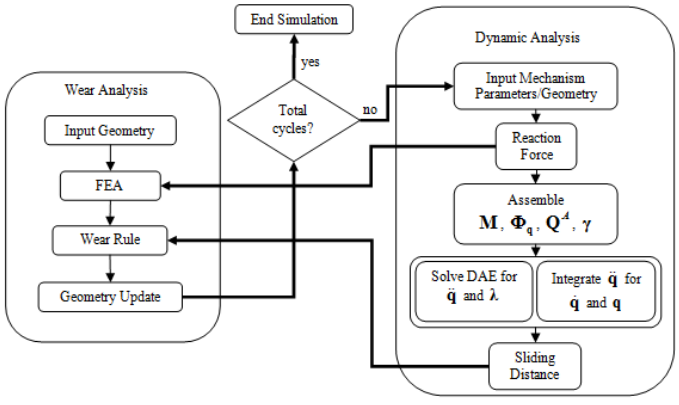

Figure 8: Integration of wear analysis into system dynamics analysis based on the contact force model

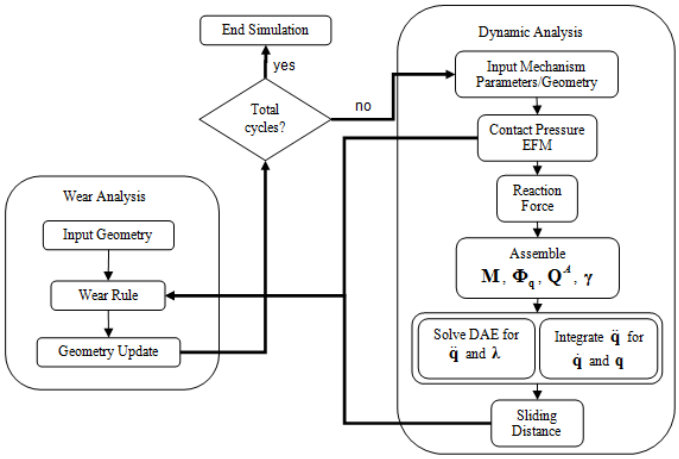

Figure 9: Integration of wear analysis into system dynamics analysis based on the EFM method.

A diagram of the slider-crank mechanism is shown in Fig. Figure 10. The mechanism was designed and constructed to allow only the joint between the crank and the follower to wear. Provisions were made to ensure that all other joints behaved as ideal joints. The components of the wearing joint were made of a hardened steel pin which is assumed to be hard enough so that no appreciable wear occurs on its surface and a PTFE bushing which is soft and experiences considerable wear. Furthermore, a spring was attached to the slider which served as a means to accelerate the wear on the bushing by increasing the joint reaction force. The joint reaction force at the joint of interest (joint between the crank and the follower) is measured using a load cell built onto a necked portion of the joint's steel pin. The load cell, provided by Deere & Company, uses two full-bridge strain gage circuits to measure the transverse shear on the pin which can then be translated into joint reaction force. Details of the corresponding instrumentation and force extraction can be found in the work of Mauntler [39-41].

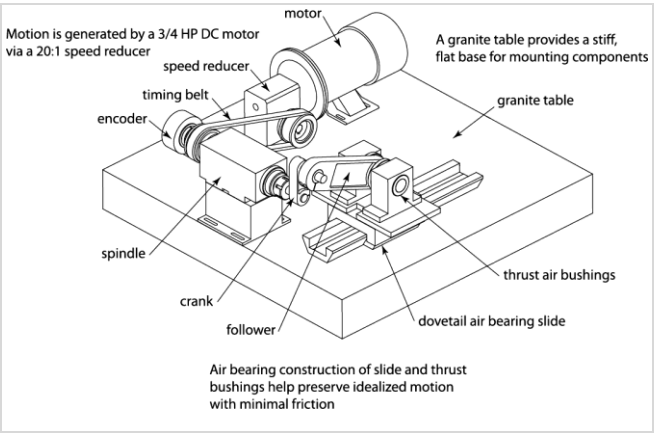

Figure 10: Slider-crank mechanism used in this study.

To allow wear debris to exit the contact area and prevent it from affecting the progression of wear, cylindrical grooves with radius of 2.29mm were machined into the bushing. A diagram of the bushing is shown in Fig. Figure 11. The dimensions and mass properties for the slider-crank are provided in Table Table 3. The dimensions, the material properties, the friction coefficient and the wear coefficient of the joint components (bushing and pin) are listed in Table

The slider-crank mechanism was operated for 21,400 cycles at a constant velocity of 30 rpm. A spring with a spring constant of 525 N/m was used. Simulations based on these conditions were conducted using the two integrated models outlined in the previous section and shown in Fig. 8 and Fig. Figure 9. For the FEM-based model the finite element model shown in Figure 12 was used. In this model, a rigid element was used to model the pin. This follows the assumption that the pin is much harder than the bushing so that it deformation would be negligible compared to that of the bushing. Furthermore, it's assumed that the pin has negligible wear and as a result retains its original shape. The bushing geometry is, however, modeled using 8-node quadrilateral element and the corresponding potential contact surface (inner bushing surface) is modeled using 3-node contact elements. The nodes on the outer surface of the bushing are constrained from translation. Contact between the two components is generated by applying the joint reaction force on the pilot node that is attached to the rigid pin element.

Table 4. Further details of the slider-crank mechanism including its construction and instrumentation can be found in the works of Mauntler et al. [39–41].

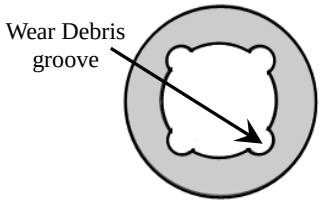

Figure 11: Bushing with debris grooves.

Table 3: Dimension and mass properties of the slide-crank mechanism

	Length (m)	Mass (kg)	Inertia x10^{-6} (kg.m^2)
Crank	0.0381	0.4045	204.0
Connecting rod	0.1016	0.8175	5500.0
Slider	-	8.5000	--

The slider-crank mechanism was operated for 21,400 cycles at a constant velocity of 30 rpm. A spring with a spring constant of 525 N/m was used. Simulations based on these conditions were conducted using the two integrated models outlined in the previous section and shown in Fig. 8 and Fig. Figure 9. For the FEM-based model the finite element model shown in Figure 12 was used. In this model, a rigid element was

used to model the pin. This follows the assumption that the pin is much harder than the bushing so that it deformation would be negligible compared to that of the bushing. Furthermore, it's assumed that the pin has negligible wear and as a result retains its original shape. The bushing geometry is, however, modeled using 8-node quadrilateral element and the corresponding potential contact surface (inner bushing surface) is modeled using 3-node contact elements. The nodes on the outer surface of the bushing are constrained from translation. Contact between the two components is generated by applying the joint reaction force on the pilot node that is attached to the rigid pin element.

Table 4: Properties of the pin and bushing

	Pin	Bushing
Bushing Inner radius	--	9.533 mm
Outer radius	9.500	15.875mm
Depth	--	13.100mm
Poisson ratio	0.29	0.38
Density	7.8 g/cm^3	2.25g/cm^3
Young's Modulus	206.8 GPa	0.500 GPa
Fric. coef. (steel-PTFE) [33]		0.13
Wear coef. (steel-PTFE) [22]		5.05x10^{-4} mm^3/Nm

The slider-crank mechanism was operated for 21,400 cycles at a constant velocity of 30 rpm. A spring with a spring constant of 525 N/m was used. Simulations based on these conditions were conducted using the two integrated models outlined in the previous section and shown in Fig. 8 and Fig. Figure 9. For the FEM-based model the finite element model shown in Figure 12 was used. In this model, a rigid element was used to model the pin. This follows the assumption that the pin is much harder than the bushing so that it deformation would be negligible compared to that of the bushing. Furthermore, it's assumed that the pin has negligible wear and as a result retains its original shape. The bushing geometry is, however, modeled using 8-node quadrilateral element and the corresponding potential contact surface (inner bushing surface) is modeled using 3-node contact elements. The nodes on the outer surface of the bushing are constrained from translation. Contact between the two components is generated by applying the joint reaction force on the pilot node that is attached to the rigid pin element.

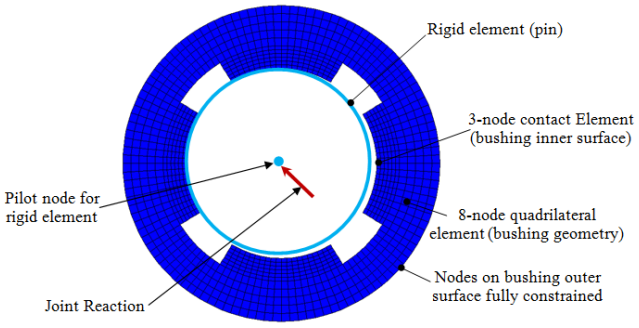

Figure 12: Finite element model for the pin and bushing.

Figures Figure 13 and Figure 14 show representative results from the initial system dynamics. Three plots of the joint reaction force from: 1) the experiment, 2) the model based on the EFM, and 3) the model based on the contact force model are shown in Fig. Figure 13. The two models, which are identical in this case, predict the joint reaction force reasonably well over the entire crank cycle except at about π radians. At this location, the measured force exhibits high frequency oscillation for a short duration. The location of these oscillations corresponds to one half of the crank rotation when the slider changes direction. It is believed that these higher order dynamics are a result of the change in the direction of the slider which most likely involves a slight rotation of the slider and thus a moment of brief impact with the sliding rail. It should be mentioned that, although the magnitude of these oscillations is large, their effects on the wear prediction is quite small. This is because the corresponding incremental sliding distance is also quite small.

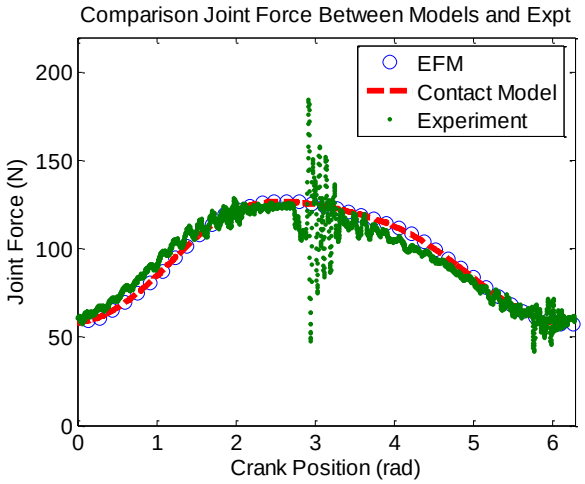

Figure 13: Comparison of the initial joint reaction force between the two models and the experiment.

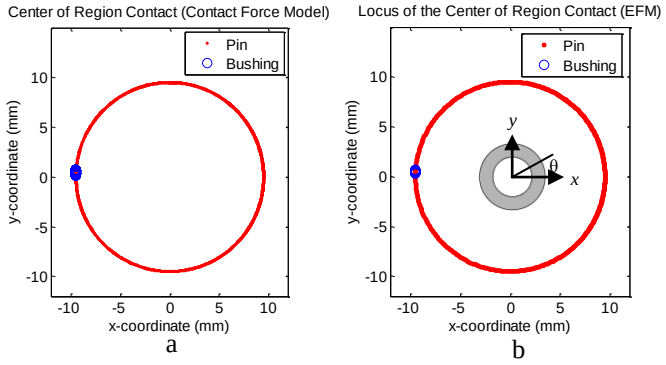

Figure 14: Locus of the center of the contact region. a) Prediction based the elastic foundation model. b) Prediction based on the contact force model.

In Fig. Figure 14 the locus of the center of the region of contact for the pin and bushing (measured for the pin and bushing centers respectively) is plotted. Figure Figure 14(a) shows the locus of points when the model based in the EFM is used. It is seen that the entire pin surface experiences contact, while the center of the region of contact on the bushing is concentrated on the left side of the bushing. This means that only one side of the bushing will experience wear and that the maximum wear will occur at the center of the region of contact. The concentration of the contact point in this location is reasonable because the spring restricts the motion of the pin relative to the bushing. FigureFigure 14(b) displays the locus of the center of the region of contact when the contact force model is used. It is clear that the two models yield nearly identical results.

The wear predicted by the contact force model (in conjunction with FEM) and the EFM models are compare in Fig. Figure 15 and Table 5. In Fig. Figure 15, it can be seen that while the FEM-based model predicts a larger maximum wear depth, the EFM has a wider base. The wider base means that a wider region in the bushing surface is worn. An interesting observation is that while the wear depth for the two models differs, their wear profile is such that the worn volume is approximately equal. This equality is a manifestation of the similarity in the force profile as shown in Fig. Figure 13. In Table 5, the computation time for the wear prediction based on the two models is compared. It can be observed that the EFM has a shorter computational time. There are two reasons for this observation: 1) evaluation of the contact pressure using EFM is inexpensive because the elastic layer is composed of a bed of springs that are assumed to be independent, and 2) in the case of the EFM-based model only one set of analyses for each cycle is required to simultaneously determine both the contact force and the contact pressure during the dynamic analysis. However, in the case of the FEM-based model the contact force is determined in the dynamic analysis which, in turn, is used to determine the contact pressure.

	FEM	EFM	Diff.
Wear Volume	106.71 mm^3	106.68 mm^3	0.02%
Max wear depth	0.4779 mm	0.4263 mm	10.70%
Computation time	11hrs	7hrs	4 hrs

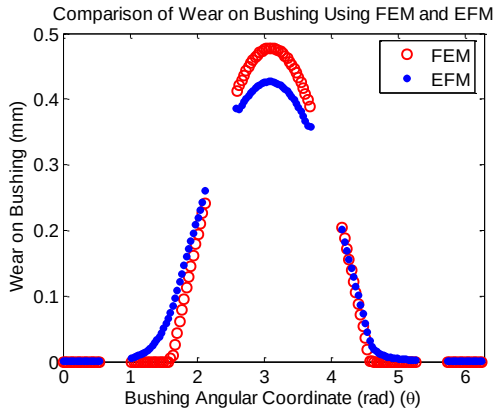

Figure 15: Comparison of the wear prediction between the models.

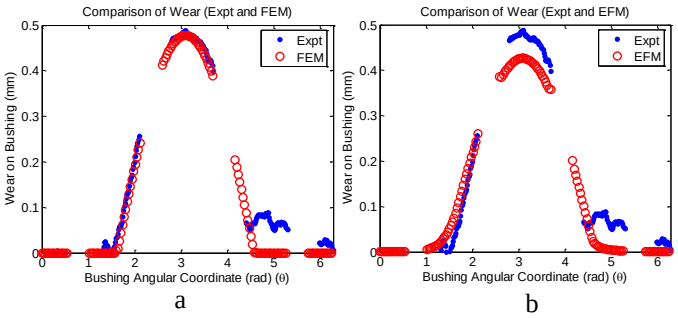

Figure 16: Comparison of the wear profile for the models and the experiment. a) Comparison between experiment and FEM. b) Comparison between experiment and EFM.

Table 5: Comparison of wear results for FEM and EFM models (21,400 crank cycles)

The wear results from experiment and simulation results for the two models are compared in Fig. Figure 16, Table 6 and Table 7. From Fig. Figure 16(a) and Table 6, it can be seen that the maximum wear depth, the wear profile and the wear volume from the experiment are accurately predicted by the FEM-based model. There is, however, a discrepancy in the range $4.5 < \theta < 6.3$ rad. This discrepancy could be attributed to errors encountered during measurement. It is possible, however, that they are the result of some wear mechanism that was not identified in the experiment.

Table 6: Comparison of wear results between test and FEM model (21,400 crank cycles)

	Expt.	Simulation (FEM)	Diff.
Worn mass	0.2616 g	0.2401 g	8.2%
Wear Volume	116.27 mm^3	106.71 mm^3	8.2%
Max wear depth	0.4850	0.4779 mm	1.5%

Table 7: Comparison of wear results between test and EFM model (21,400 crank cycles)

	Expt.	Simulation (EFM)	Diff.
Worn mass	0.2616 g	0.2400 g	8.2%
Wear Volume	116.27 mm^3	106.68 mm^3	8.2%
Max wear depth	0.4850	0.4263 mm	12.1%

In the case of the EFM model, the wear profile and the maximum wear depth are incorrectly predicted as shown in Fig. Figure 16(b) and Table 7. The location of maximum wear and the wear volume are, however, correctly predicted as expected.

7. CONCLUDING REMARKS

The objective of this work was to present a comparison between two models that can be used to analyze multibody systems with joint wear. The comparison was based on wear results of an experimental slider-crank mechanism that was built to encourage wear at a single joint (a revolute joint between the crank and the follower). Quantities that were considered in the comparison included the joint reaction, the contact/wear location and wear amount on the bushing.

For the initial dynamics the two models provided reasonably accurate prediction of the contact force. This indicates that the system dynamics are insensitive to the contact model used. The two models also produced identical prediction for the location of maximum wear, which was verified to be the correct location through the corresponding experiment. Although this location was correctly predicted by both models, only the FEM-based model gave an accurate prediction of the wear profile and maximum wear depth. Prediction from the FEM-based model differed by 6.7% from experiment, while the prediction from the EFM model differed by 12.1% from experiment. The difference in the wear depth prediction between the FEM- and EFM-based models is attributed to the assumption that the springs forming the elastic foundation are independent (no shear force between the springs). As was mentioned earlier, the consequence of this assumption is that the model does not account for how pressure applied at one location affects the deformation at other locations [42]. This is contrary to what is experienced in elastic contact where the displacement at one location is a function of the pressure applied at other locations. Thus as is observed, the FEM-based model provides a better prediction of the wear depth. It should, however, be noted that, while the predictions on the wear profile differed, the wear volume predictions of the two models were identical and reasonably close to the experimental wear volume (8.2 %).

Despite the poor prediction on the wear profile and maximum wear depth, the EFM-based model had a shorter computation time. The experiment took about 12 hours (excluding construction and setup time) and FEM-based model took 11 hours, while the EFM-based model took only 7 hours to complete. The speed of the EFM-based model is associated with the assumption that the springs in the elastic foundation model are independent and the fact the only one analysis is required to determine both the contact pressure distribution and the joint reaction.

From the comparison between the results of the two models and between the results of the two models and the experiment, the following conclusions can be made: 1) the two procedures can accurately predict the contact force, the contact locations and the wear volume, 2) the FEM-based procedure is a better predictor of maximum wear depth and the wear profile than the EFM-based procedure, and 3) the EFM model is computationally less expensive than the FEM-based model.

It can be concluded that the FEM-based procedure is preferred for the analysis of multibody systems with joint wear when the computational cost is not an issue. If the cost is a concern, however, and only qualitative information about the system is needed, then the EFM-based procedure is a suitable choice. Other scenarios will require a compromise on either accuracy or computational costs.

NOMENCLATURE

A	: Contact area
A_E	: Extrapolation factor
δ	: Penetration
e_r	: Coefficient of restitution
E	: Young's modulus
F_N	: Normal force in the contact interface
h	: Wear depth
k	: Dimensioned wear coefficient
K	: Elastic constant
$\boldsymbol{\lambda}$	: Vector of Lagrange multipliers
$\mathbf{M}$	: Mass matrix
p	: Contact pressure
$\mathbf{q}$	: Position vector
$\mathbf{Q_A}$	: Vector of applied loads
s	: Sliding distance
t	: Time
υ	: Poisons ratio
$\boldsymbol{\Phi}$	: Constraint vector
$\boldsymbol{\Phi}_\mathbf{q}$	: Jacobian matrix
ω	: Crank velocity

ACKNOWLEDGMENTS

The authors gratefully acknowledge support by the National Science Foundation (DMI-0600375) and Deere & Company.

REFERENCES

[1] Archard, J.F., 1953, "Contact and rubbing of flat surfaces," Journal of Applied Physics, 24, pp. 981–988.

[2] Hugnell, A.B.-J., Andersson, S., 1994, "Simulating follower wear in a cam-follower contact," Wear, 179 pp. 101–107.

[3] Hugnell, A.B.-J., Bjorklund, S., Andersson, S., 1996, "Simulation of the Mild Wear in a Cam-Follower Contact with Follower Rotation," Wear, 199, pp. 202–210.

[4] Sawyer, W.G., 2001, "Wear Predictions for a Simple-Cam Including the Coupled Evolution of Wear and Load," Lubrication Engineering, pp. 31-36.

[5] Dickrell III, D.J., Dooner, D.B., Sawyer, W.G., 2003, "The evolution of geometry for a wearing circular cam: analytical and computer simulation with comparison to experiment," ASME Journal of Tribology 125, pp. 187–192.

[6] Mukras, S., Kim, N.H., Sawyer, W.G., Jackson, D.B., Bergquist, L.W., 2009, "Numerical integration schemes and parallel computation for wear prediction using finite element method," Wear, 266 pp. 822–831.

[7] Flodin, A., Andersson, S., 2001, "A simplified model for wear prediction in helical gears," Wear 249, pp. 285–292.

[8] Flodin, A., Andersson, S., 1997, "Simulation of Mild Wear in Spur Gears," Wear 207, pp. 16–23.

[9] Brauer, J., and Andersson, S., 2003, "Simulation of Wear in Gears with Flank Interference-a Mixed FE and Analytical Approach," Wear, 254, pp. 1216–1232.

[10] Maxian, T.A., Brown, T.D., Pedersen, D.R., Callaghan, J.J., 1996, "A Sliding-Distance Coupled Finite Element Formulation for polyethylene wear in total hip arthroplasty, " Journal of Biomechanics, 29, pp. 687–692.

[11] Bevill, S.L., Bevill, G.R., Penmetsa, J.R., Petrella, A.J., Rullkoetter, P.l J., 2005, "Finite element simulation of early creep and wear in total hip arthroplasty," Journal of Biomechanics, 38, pp. 2365–2374.

[12] Blanchet, T.A., 1997, "The Interaction of Wear and Dynamics of a Simple Mechanism," Journal of Tribology, 119, pp. 597–599.

[13] Sawyer, W.G., Diaz, K.I., Hamilton, M.A., Micklos, B., 2003, "Evaluation of a Model for the Evolution of Wear in a Scotch-Yoke Mechanism," ASME, 125, pp. 678–681.

[14] Dickrell, D.J., Dooner, III,D.B., and Sawyer, W.G., 2003, "The evolution of geometry for a wearing circular cam: analytical and computer simulation with comparison to experiment," ASME Journal of Tribology 125, pp. 187–192.

[15] Mukras, S., Mauntler, N., Kim, N.H., Schmitz, T.L., Sawyer, W.G., 2008, "Dynamic Modeling of a Slider-Crank Mechanism with Joint Wear," Paper No. DETC2008-49244, ASME 32nd Annual Mech. and Robo. Conference, N.Y., N.Y.

[16] Flores, P., 2009, "Modeling and simulation of wear in revolute clearance joints in multibody systems," Mechanism and machine theory, 44(6), pp. 1211–1222.

[17] Bei, Y., and Fregly, B.J., 2004, "Multibody dynamic simulation of knee contact mechanics," Medical Engineering and Physics 26, pp. 777–789.

[18] Fregly, B.J., Sawyer, W.G., Harman, M. K., and S. Banks, A., 2005, "Computational wear prediction of a total knee replacement from in vivo kinematics," Journal of Biomechanics, 38, pp. 305–314.

[19] Podra, P., and Andersson, S., 1997, "Wear simulation with the Winkler surface model," Wear, 207, pp. 79–85.

[20] Podra, P., and Andersson, S., 1999, "Simulating sliding wear with finite element method," Tribology International, 32, pp. 71–811.

[21] Kim, N.H., Won, D., Burris, D., Holtkamp, B., Gessel, G.R., Swanson, P., Sawyer, W.G., 2005, "Finite element analysis and experiments of metal/metal wear in oscillatory contacts," Wear, 258, pp 1787–1793.

[22] Schmitz, T.L., Action, J.E., Burris, D.L., Ziegert, J.C., Sawyer, W.G., 2004, "Wear-Rate Uncertainty Analysis," ASME Journal of Tribology, 126(4), pp. 802–808.

[23] Yang, L.J, 2005, "A test methodology for determination of wear coefficient," Wear, 259 1453–1461.

[24] Nikravesh, P.E., 1988, Computer-Aided Analysis of Mechanical System, Prentice-Hall, Englewood Cliffs, NJ.

[25] Haug, E. R., 1989, Computer-Aided Kinematics and Dynamics of Mechanical Systems, Allyn and Bacon, Needham Heights, US-MA.

[26] Flores P., 2004, "Dynamic Analysis of Mechanical Systems with Imperfect Kinematic Joints," Ph.D. Thesis, Minho University (Portugal), Guimarães

[27] Ravn, P., 1998, "A Continuous Analysis Method for Planar Multibody Systems with Joint Clearance," Multibody Systems Dynamics, Kluwer Academic Publishers, 2, pp. 1–24.

[28] Flores, P., Ambrósio, J., 2004, "Revolute Joints with Clearance in Multibody Systems," Computers and Structures, 82, pp. 1359–1369.

[29] Hunt, K.H., Crossley, F.R., 1975, "Coefficient of restitution interpreted as damping in vibroimpact," Journal of Applied Mechanics, 7, pp. 440–445.

[30] Dubowsky, S., Freudenstein, F., 1971, "Dynamic Analysis of Mechanical Systems with Clearances Part1: Formulation of Dynamic model," Journal of Eng. for Industry, pp. 305–309.

[31] ESDU-78035 Tribology Series. Contact phenomena I: stresses, deflections and contact dimensions for normallyloaded unlubricated elastic components. London: Engineering Sciences Data Unit; 1978.

[32] Schwab, A. L., Meijaard, J.P., Meijers, P., 2002, "A Comparison of Revolute Joint Clearance Models in the Dynamic Analysis of Rigid and Elastic Mechanical Systems," Mechanisms and Machine Theory, 37, pp. 895–913.

[33] Schmitz, T.L., Action, J.E., Zigert, J.C., Sawyer, W.G., 2005, "The Difficulty of Measuring Low Friction: Uncertainty Analysis for Friction Coefficient Measurment," Journal of Tribology, 127, pp. 673–678.

[34] Johnson, K.L., 1985, Contact mechanics, Cambridge University Press, Cambridge.

[35] Blankevoort, L., Kuiper, J.H., Huiskes, R., Grootenboer, H.J., 1991, "Articular contact in a three-dimensional model of the knee," Journal of Biomechanics, 24, pp. 1019–1031.

[36] Pandy, M.G., Sasaki, K., Kim, S., 1997, "A three-dimensional musculoskeletal model of the human knee joint. Part 1: theoretical construction," Computer Methods in Biomechanics and Biomedical Engineering, 1, pp. 87–108.
[37] An, K.N., Himenso, S., Tsumura, H., Kawai, T., Chao, E.Y.S., 1990, "Pressure distribution on articular surfaces: application to joint stability analysis," Journal of Biomechanics, 23, pp. 1013–1020.
[38] Li, G., Sakamoto, M., Chao, E.Y.S., 1997, "A comparison of different methods in predicting static pressure distribution in articulating joints," Journal of Biomechanics, 30, pp. 635–638.
[39] Mauntler N., 2009, "Kinematic and Dynamic Behavior of a Wearing Joint in a Crank-Slider Mechanism," Ph.D. Thesis, University of Florida (USA), Gainesville.
[40] Mauntler, N., Kim, N.H., Sawyer, W.G., Schmitz, T.L., 2007, "An instrumented crank-slider mechanism for validation of a combined finite element and wear model," Proceedings of 22nd Annual Meeting of American Society of Precision Engineering, October 14–19, Dallas, Texas.
[41] Mauntler, N., Mukras, S., Kim, N.H., Schmitz, T. L., Sawyer, W. G., 2009, "An Instrumented Crank-Slider Mechanism for Wear Testing," STLE 64th Annual Meeting, Lake Buena Vista, Florida.
[42] Söderberg A. and Björklund S., 2008, "Validation of a Simplified Numerical Model," Tribology International, 41, pp. 926–933.
[43] Johnson, K. L., 1985, "Contact Mechanics," Cambridge University Press, New York.
[44] Thornton, C., 1997, "Coefficient of Restitution for Collinear Collisions of Elastic-Perfectly Plastic Spheres," ASME J. Appl. Mechanics, 64, pp. 383-386.
[45] Katta, R. R., Polycarpou, A. A., Hanchi, J. V., and Crone, R, M., 2009, "High Velocity Oblique Impact and Coefficient of Restitution for Head Disk Interface Operational Shock," ASME J. Tribol., 131, 021903.